

Pulsed glow discharge in thin-walled metallic hollow cathode. Analytical possibilities in atomic and mass spectrometry

S. Potapov,^a E. Izrailov,^a V. Vergizova,^{a,b} M. Voronov,^{a,b} S. Suprunovich,^{a,b}
M. Slyadnev^{a,b} and A. Ganev^{*a,b}

^aLumex Ltd., Moskovskij pr. 19, St. Petersburg, Russia. E-mail: potapovsv@lumex.ru;

Fax: +7 812 1186865; Tel: +7 812 118 6860

^bDepartment of Chemistry, St. Petersburg State University, Universitetskij pr.2, St. Petergoff,

St. Petersburg, Russia. E-mail: root@aga.chri.spb.ru; Fax: +7 812 4286739;

Tel: +7 812 4284088

Received 6th January 2003, Accepted 11th March 2003

First published as an Advance Article on the web 23rd April 2003

In this article investigation of atomization and ionization processes in pulsed glow discharge with atomic absorption and mass spectrometry is reported. It was shown that sample sputtering and atomization in a thin-walled metallic hollow cathode (TMHC) is highly efficient in pulsed glow discharge plasma. Using a TMHC as an atomizer with a Zeeman AAS system a background absorption influence for samples with high matrix concentration was significantly reduced compared with graphite furnace AAS. This effect is attributed to the high efficiency of dissociation of matrix components in pulsed glow discharge. TMHC was also used as an ion source for an analytical system with time-of-flight mass-spectrometry (TOF-MS). Ionization processes in pulsed glow discharge were theoretically simulated using modified algorithms and the results of the simulation were experimentally confirmed. It was shown that Penning ionization significantly contributes to ionization yield even after pulsed discharge termination. Sample sputtering dynamics for different discharge regimes were explained and transportation processes from TMHC to TOF-MS were optimized. Limits of detection for Cd and Cu were 20 and 15 ng l⁻¹, respectively.

Introduction

Glow discharge (GD) has been used as an atom and ion source in atomic spectrometry for the last 50 years. The relative simplicity, low cost of operation and reliability of the GD source make it a very attractive tool for both optical spectroscopy and mass spectrometry.^{1–4} Currently, glow discharge mass spectrometry (GD-MS) is recognized as one of the most powerful and efficient techniques for the direct elemental analysis of solids.^{5,6} Moreover, successful attempts to apply GD-MS to composition analysis have been carried out recently; the molecular integrity of the analyte species introduced into the glow discharge ion source can be at least partly retained due to Penning ionization.⁷

Three different types of the GD ion source are used in mass spectrometry at present—direct current (dc), radiofrequency (rf) and microsecond pulsed (μ s-pulsed) discharge. Applications of dc-GD-MS for the analysis of conducting materials are described in refs. 8–13. However, the analysis of non-conducting materials by dc-GD-MS is especially difficult due to charge-up effects on the sample surface. In order to extend the range of analyzed samples to non-conducting materials two different approaches are usually applied. The first approach is to prepare a cathode by mixing of analyzed sample with a conducting component, such as high-purity graphite or metal powder.¹⁴ The second way is to insert a secondary cathode into the discharge cell, which produces a thin conducting layer on the sample surface in the course of sputtering with Ar⁺ ions of plasma gas.^{15,16} In contrast to dc-GD-MS, rf and μ s-pulsed GD-MS are applicable to the analysis of conducting, semi-conducting and non-conducting samples. Detection limits for rf and dc ion sources are almost equal.¹⁷ For μ s-pulsed GD substantially higher sputtering rates and, in consequence, lower detection limits are reported.^{18,19}

In modern analytical laboratories there is a requirement for

analysis of both solids and liquids. There are some attempts to develop combined GD-ICP-MS instrumentation with exchangeable ion sources^{20–23} in order to analyze both kinds of samples. As an alternative, a number of researchers used GD devices for indirect analysis of liquid samples by the sputter atomization of solution residues.^{24–30} The solution under investigation (1–100 μ l) is placed on a planar cathode or inside the hollow cathode surface and dried directly or by infrared heating. This procedure can be applied in atomic absorption,^{24,25} emission,^{26,27} fluorescence,²⁸ resonance-ionization spectroscopy,²⁹ or mass spectrometry.^{30,31}

In the case of solution analysis, however, the presence of water in “dry residue” may lead to essential deterioration of the analytical signal, especially in mass spectrometry.^{32,33} There are some methods to avoid interferences induced by water: liquid chromatographic separation of analyte from solvent before introduction into a GD source;³⁴ application of electric arc pretreatment eliminating water from residue; or using an argon–hydrogen/argon–methane mixture as the discharge gas in a GD cell.³⁵

In almost all applications of GD in atomic spectrometry a Grimm-type glow discharge is used.³⁶ This type of glow discharge is the most-used source for atomic emission spectroscopy owing to its good precision and relatively small matrix effects,³⁷ but it is rarely applied for atomic absorption.³⁸ Other examples of GD applications for liquid samples analysis, such as hot hollow cathode atomization with emission spectroscopy³⁹ and laser fluorescent spectrometry⁴⁰ detection were also demonstrated.

The advantages of GD sources with pulsed discharge have been shown by several research groups. High current density and high energy of the sputtering ions result in a high rate of sputtering of a thin layer of sample residue, which in its turn is higher than the rate of metal wall sputtering. Time-of-flight mass-spectrometry (TOF-MS) especially benefits from utilizing

a pulsed GD ion source. In this case, for ions production, the very effective pulsed Penning ionization of sample atoms provides a high degree of ionization ($\approx 10\%$). High ion detection efficiency in the orthogonal acceleration configuration, together with temporal discrimination between sample ions and discharge gas ions, improves the analytical performance of the TOF-MS method.

As has been shown for the thin-walled metallic hollow cathode (TMHC) atomizer, sputtering of dry residues is appreciably increased in the pulsed glow discharge at relatively high currents (up to 4 A). This effect is caused by increase in current density, ion energy and by heating of the TMHC up to 1200–1400 °C.^{25,29} Low bonding energy between the residue and the cathode surface results in high efficiency of sample sputtering (the probability of sputtering is $0.5\text{--}40\text{ s}^{-1}$) and ionization in the hollow cathode and allows determination of the elements in solutions with detection limits within ppb (for AAS) and ppt (for TOF-MS) ranges. The high rate of sputtering is determined by an ionic-thermal sputtering mechanism of residue.^{25,29} It is also worthy of note that low rates of discharge gases consumption ($2\text{--}10\text{ ml min}^{-1}$, $p = 1\text{--}5\text{ Torr}$) and low average discharge power (60–200 W) allow the use of pulsed GD sources in mobile analytical spectrometers designed for field and on-site applications.

This article presents theoretical and experimental investigations of atomization and ionization processes in pulsed thin-walled metallic hollow cathode glow discharge. There are reported analytical applications of TMHC with two detection systems—Zeeman atomic absorption spectrometry with high frequency modulated light polarization (TMHC-ZAAS-HFM) and time-of-flight mass spectrometry (GD-TMHC-TOF).

Theory

The theoretical investigation is intended for studying the dynamics of sputtering, ionization and transportation processes for a sample in glow-discharge plasma. This simulation provides the possibility of optimization of discharge parameters and for obtaining better analytical results. Computer simulation also allows estimation of the influence of matrix elements on sputtering rate and ions counts. The calculations are based on a self-consistent description of plasma particle distributions and dynamics (electrons, ions, sample atoms, *etc.*) and electrical field configuration. Input parameters of the model are discharge geometry, applied voltage as a function of time, gas pressure and temperature. The simulation results are dynamic curves of concentration for all particles under investigation, their space distributions and discharge current.

The discharge geometry scheme is as follows: the cathode is made as a niobium cylinder with a bottom. A sample dry residue is assumed to be homogeneously deposited on the inner cylinder surface. The sampler is a plate with an orifice for ion extraction. The basic discharge gas is Ar.

Our model consists of two parts: the pulsed discharge and afterglow. The space distributions of all kinds of particles obtained at the end of discharge simulation are used as input data for afterglow simulation. At the first stage the plasma is formed due to applied high voltage and at the second stage the plasma has decayed.

During the plasma formation stage high voltage (up to 2 kV) is applied to the cathode. Particle movement and electrical field configuration are calculated self-consistently. Particle movement is simulated by the Monte-Carlo technique. Electrons, as well as argon and sample ions, are taken into account in simulating electrical dynamics at the plasma formation stage. The Monte-Carlo method is also applied to Ar metastable atoms, Ar fast neutral atoms and sample atoms and ions to describe sample sputtering and ionization processes. The rates of various reactions are calculated during the movement of

particles, *i.e.*, electron impact ionization, ion impact ionization, sputtering, Penning ionization and elastic collisions are taken into account. We do not take into account other sample ionization processes because electrons and ions are not powerful enough to produce impact ionization. Furthermore, other ionization processes like asymmetric charge transfer have a small cross-section.

A flow-chart of algorithm of Monte-Carlo simulation will be presented in detail elsewhere.[†] Briefly, the Monte-Carlo simulation technique is based on application of basic Newton's laws of motion to all particles and calculation of collision probability by means of known process cross-sections, which is also generally referred as the "particle-in-cell" approach. In the present model we use the Monte-Carlo simulation self-consistently with the discharge electrical field calculation. It allows us to describe actual electrical dynamics of the discharge.

The model demands that the electrical field configuration should be recalculated very often (after movement of every charged particle) because the amount of charged particles in the model is relatively small (just about 30000) and movement of every charged particle can induce appreciable modification of the field. Originally the electrical potential configuration should be obtained from the Poisson equation:

$$\Delta V = -4\pi\rho$$

where V is electrical potential and ρ is the charge density. Unfortunately, this equation solving procedure is too time-consuming to be applied after movement of every charged particle. Moreover, this procedure becomes unstable because relatively small amounts of charged particles lead to a small field fluctuations. As an alternative we employed phenomenological laws of the electrical potential behavior in plasma, such as cathode dark space thickness dependence of charged particles density and voltage dependence of the total number of charged particles in a discharge. We assumed that the cathode dark space thickness is determined by Debye radius and related with charged particles density as:

$$L = (kT_e/4\pi ne^2)^{1/2}$$

where L is the cathode dark space thickness and n is the ion density. This dependence provides a negative feedback between the electrical field configuration and the rates of charged particles origination and elimination. In fact, if present ion density is higher than stationary ion density: the field is formed to stimulate ion elimination at the cathode and *vice versa*. The dependence between the voltage and plasma total charge is assumed to be proportional:

$$V \propto Q$$

where V is the electrical potential and Q is the plasma total charge. This dependence provides a negative feedback between the electrical field configuration and balance of electrons and ion elimination rates (*i.e.* electrical current). In fact, if the present ion current exceeds the electron current, the field is formed to accelerate electrons flow to the cathode and decelerate ion flow.

At the plasma decay stage no voltage is applied to the cathode. We assume that at this stage the electrons are not powerful enough to produce ions and metastable Ar atoms efficiently. Therefore, we solved the balance equation for all kinds of particles together with the Poisson equation for electrical field:

[†]Article is in preparation for submission to *JAAS*.

$$\begin{aligned} \frac{\partial n_i}{\partial t} - D_i \Delta n_i - \mu_i \nabla V &= 0 & n_i|_{\partial} &= 0 \\ \frac{\partial n_c}{\partial t} - D_c \Delta n_c + \mu_c \nabla V &= 0 & n_c|_{\partial} &= 0 \\ \frac{\partial n_{Ar}}{\partial t} - D_{Ar} \Delta n_{Ar} &= -K_p n_{Ar} n_s & n_{Ar}|_{\partial} &= 0 \\ \frac{\partial n_s}{\partial t} - D_s \Delta n_s &= -K_p n_{Ar} n_s & n_s|_{\partial} &= 0 \\ \frac{\partial n_{si}}{\partial t} - D_{si} \Delta n_{si} - \mu_{si} \nabla V &= K_p n_{Ar} n_s & V|_{\partial} &= 0 \end{aligned}$$

$$\Delta V = -4\pi e(n_i - n_c)$$

where n_i is Ar ion density, n_c is the electron density, n_{Ar} is Ar metastable atoms density, n_s is sample atoms density, n_{si} is sample ions density and V is electrical potential. A boundary condition for the sample atoms includes a flux of sample atoms reflected from the walls²⁹ (it is assumed that the sample atoms reflection probability is 0.5).⁴³

Calculated space-averaged densities of particles at the end of discharge pulse are presented in Table 1. As can be seen from Table 1, the density of metastable Ar atoms at the beginning of afterglow is much greater than the density of Ar ions, hence an ion–electron impact recombination production term in the equation for Ar metastable atoms was neglected and the recombination cannot influence metastable Ar atoms density and Penning ionization rate significantly. In fact, the main source for metastable Ar atoms in afterglow is pulsed discharge.

In contrast to other authors^{41–47} studying the glow discharge by computer simulation, we calculated all particle dynamics using only the Monte-Carlo technique rather than a separated simulation algorithm on the Monte-Carlo and fluid models. This approach allowed us to directly calculate electron and ion movement and avoid particle separation into fast and slow species. Besides, our model deals with the cylindrical shape of the cathode. Moreover, our calculations make a point of the sample behavior dynamics rather than of static distribution of the cathode substance.

Sputtering processes in the model are described by ionic–thermal sputtering mechanism, which is explained in detail elsewhere.^{25,29} It has been shown that the sputtering probability is strongly dependent on impacting particle mass and energy (*i.e.* cathode potential), and the TMHC temperature.

There are two ways to achieve high atomization probability (of order 1–10 s⁻¹): to increase the cathode potential and, correspondingly, the ions energy, or to increase the mass of impacting ion, *i.e.*, to use heavy noble gases (such as Kr or Xe) or heavy elements with low ionization potential (for example Cs, Ba), introduced together with the sample.

When the sample with a complex matrix is analyzed, injection of elements with low ionization potential allows us to avoid the condition where the predominant ionic flow to the TMHC surface is defined by lightweight ions of the matrix that could reduce the sputtering probability.

Table 1 Calculated space-averaged densities of particles at the end of the plasma formation stage (cm⁻³)

Ar metastable atoms	1.2 × 10 ¹⁴
Ar ions	1.6 × 10 ¹³
Cu atoms	7.6 × 10 ¹²
Cu ions	3.3 × 10 ¹¹
Ar fast atoms	1.9 × 10 ¹³

Experimental

Pulsed discharge in thin-walled metallic hollow cathode with Zeeman high frequency modulated light polarization spectrometry

An experimental set-up for the TMHC-ZAAS-HFM method and basic operation principles were described in detail elsewhere.^{25,29} The key differences between the reported system and the present instrument are the following. A quartz discharge camera was used instead of a stainless steel discharge tube and the electromagnet was replaced by a rare-earth elements magnet with constant field strength of 3.5 kOe. The power unit was improved in order to supply pulses of 2000 V, 10–200 μs and 1–5 kHz. The upper side of TMHC cylinder was directly connected with niobium capillary for sample injection. The discharge camera was installed in the commercially available ZAAS spectrometer (MGA-915, Lumex, St. Petersburg, Russia) which had been modified to combine light sources, monochromator, detectors, gas vessel, vacuum pump, power supply and control electronics in a single unit.

All modifications were made in order to create a mobile ZAAS instrument with automated sample injection system suitable for on-site analysis. As was shown earlier, the low power consumption of the TMHC atomizer and low gas flow rate allow operation of the TMHC-ZAAS spectrometer in field conditions.

The sample injection system has been specially designed to combine sample loading into TMHC and Ar flowing during discharge through the Nb capillary and is described in the next section. The TMHC discharge operation conditions and analytical procedures are summarized in Table 2.

Pulsed discharge in thin-walled metallic hollow cathode with time-of-flight mass spectrometry

The experimental system based on TMHC glow discharge ion source and time-of-flight mass spectrometer is shown in Fig. 1. The ion source with a coaxial arrangement was designed for analyzing of liquid samples (5–20 μl) after drying them to residue. The niobium capillary (for a few experiments a stainless steel capillary was used) was welded to the bottom of the thin-walled metallic hollow cathode, as is shown in Fig. 1. The capillary serves for injection of discharge gas (Ar, Kr or Ar–He mixture) and liquid sample into the TMHC. In the experiments two types of sampler were used: the first type was planar and the second type was conical in configuration (see Fig. 1).

The pressure ratio between the first (discharge cell) and the second (space between sampler and skimmer) vacuum stages was approximately 100:1 for the pumping rate of 70 l s⁻¹ at the second stage. The pressure in the time-of-flight tube was within the range (1–3) 10⁻⁵ Torr. The TOF direction in the spectrometer was orthogonal to ion beam axis. The repelling volume is bounded by a push-out electrode (POE) and a grid,

Table 2 TMHC-ZAAS operating and analytical conditions

<i>General conditions—</i>			
Discharge voltage	2000 V		
Discharge current	Up to 1 A		
Discharge pressure	15–30 Torr		
<i>Analytical conditions—</i>			
	Cu	Pb	Ag
Pulse frequency	1 kHz	5 kHz	3 kHz
TMHC temperature	1500 K	1300 K	1300 K
Pulse duration	60 μs	200 μs	100 μs
Atomization time	6 s	4 s	1.5 s
<i>Sampling procedures—</i>			
Drying time	150 s		
Analysis time	180 s		
Sample volume	10 μl		

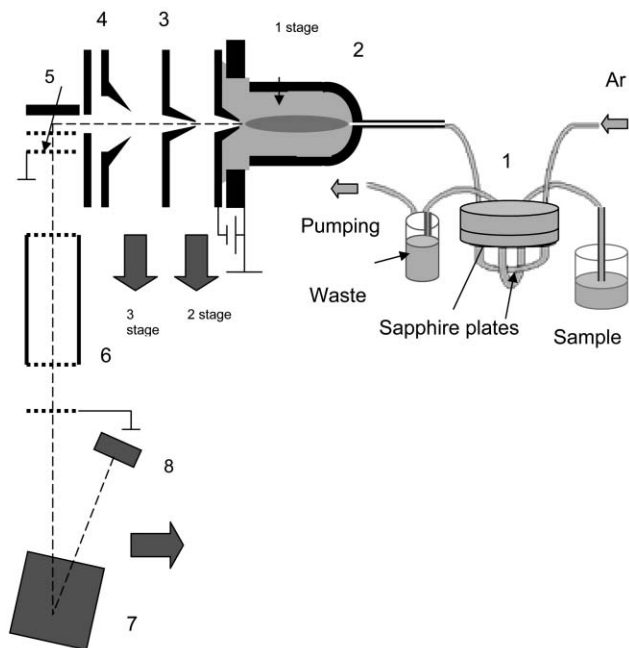


Fig. 1 Schematic drawing of experimental set-up for TMHC with TOF-MS. 1, Sampler; 2, TMHC; 3, diaphragm; 4, entrance slit; 5, push out electrode; 6, acceleration tube; 7, reflectron; 8, MCP (multi-channel plate) detector.

Table 3 TMHC-TOF-MS operating condition

Discharge voltage	2000 V
Discharge current	up to 4 A
Sampler voltage	0–20 V
Skimmer voltage	0–1800 V
Lens voltage	200–2000 V
Repelling pulse voltage, POE	300 V
Repelling pulse voltage, grid	150 V
Flight tube voltage	2000 V
MCP voltage	1800–2000 V
Ionization pulse duration	10–80 μ s
Repelling pulse duration	0.5–2.5 μ s
Frequency of discharge pulses, <i>F</i>	100–10000 Hz
Discharge pressure, Ar	0–1.5 Torr
Discharge pressure, He	0–7 Torr
Sample volume	5–50 μ l
Orifice diameter	0.6–0.8 mm
Slit	0.2 mm

as is indicated in Fig. 1. A flight tube with high voltage and a reflectron are used in TOF. Two microchannel plates were used as a detector. The voltages of the grids and flight tube and other parameters of spectrometer are presented in Table 3.

The system for liquid sample injection in TMHC from the open sample cell (pressure 1 atm) to the closed discharge cell (pressure \approx 1 Torr) was specially designed. The system (see Fig. 1) includes two sapphire plates with high quality polished surfaces ($\lambda/5$) and four orifices drilled in each plate. Two crossing loops (the first loop serves as a transit loop, the second one is intended for determination of sample volume) were connected to one of the plates. Capillaries from another plate were connected to the sample cell, waste cell, Ar gas inlet and TMHC. During operation the sample loading and sample injection steps were performed sequentially. At the sample loading stage, the sample loop capillary was filled with sample solution that passed from the open sample cell, through sapphire plates into the waste cell. Then one of the plates was rotated relative to the other, so the filled loop was connected with the Ar gas inlet and the cathode outlet. At the sample injection stage the sample was pushed out of the loop by Ar moderate pressure and deposited into the TMHC discharge cell.

After injection the sample (up to 50 μ l) was dried for 3–4 min by Ar lamp emission (through the quartz wall of the discharge cell). After drying the sample residue was sputtered and ionized by pulsed discharge.

Results and discussion

Atomization in TMHC with ZAAS detection

One of the important analytical characteristics of the TMHC as an atomizer is the atomization rate. The mechanisms of solution dry residue sputtering in TMHC and sample atomization in discharge plasma were discussed in the details in our previous publication.^{25,29} It has been shown that the atomization mechanism has a complex combined character. Compounds with relatively low boiling temperature are evaporated from the atomizer surface and transferred into the gaseous phase before dissociation on the atomizer surface. Then they are dissociated in the glow discharge plasma at collision with high-energy ions, electrons and metastable atoms of the discharge gas. Atomization of the compounds with high boiling temperature is defined by two factors: TMHC temperature and ion impact. It has been shown that in this case the atomization process is defined mainly by the ionic bombardment of the TMHC surface with high-energy gas ions but the temperature plays the secondary part. The sputtering in a TMHC glow discharge atomizer was described by an ionic-thermal mechanism considered in detail elsewhere.^{25,29}

To study the influence of matrix components on TMHC atomization performance model samples were analyzed in 3% NaCl solution. Fig. 2 shows the atomization profiles for samples containing 0.2 ng of Ag, 0.4 ng of Pb and 300 μ g of NaCl. Matrix effects (*i.e.*, background absorption and incomplete atomization of the analyte) can be studied in experiments with such samples that closely imitate marine water, human urine or blood plasma in salt content. As can be

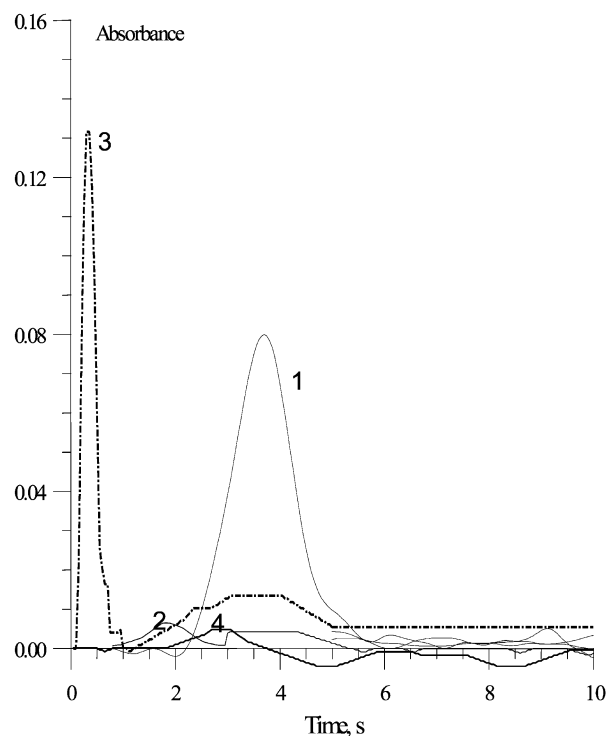


Fig. 2 Atomization profiles and background signals as a function of time for 0.4 ng of Pb (curves 1 and 2, respectively) and 0.2 ng Ag (curves 3 and 4, respectively) with 300 μ g of NaCl (10 μ l of 3% solution) added to the sample.

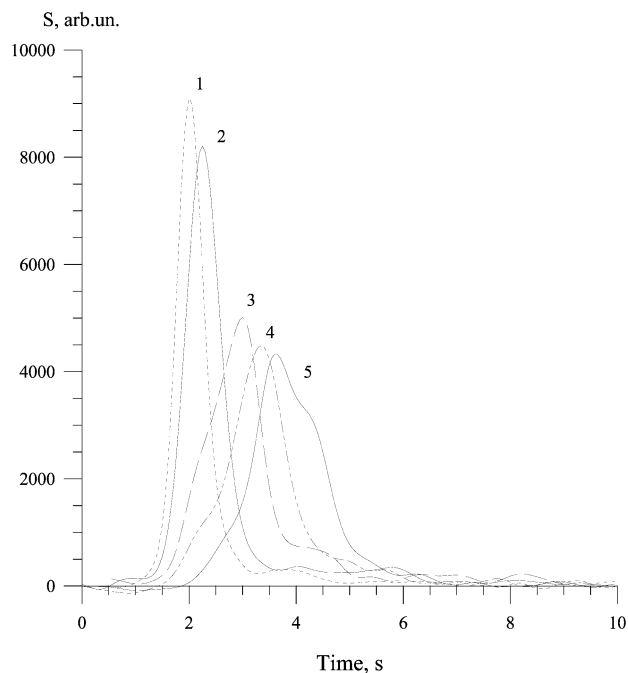


Fig. 3 Atomization profiles for 0.3 ng Ag with different amount of NaCl added to the sample: curves (1), 0 µg; (2), 1 µg; (3), 4 µg; (4), 20 µg; (5), 200 µg.

seen from Fig. 2, the background absorption signal does not exceed 0.15 units of absorbance for Pb while the background absorption is close to zero for Cu. This finding is evidence of the high degree of dissociation of the NaCl molecules in the discharge plasma.

However, the value of the analytical signal S_i for pure solutions and for solutions contained NaCl within the range 0.3–200 µg was different for every element under study. Atomization profiles for Ag are shown in Fig. 3 for the cases when a different amount of NaCl was added to the sample. As can be seen from Fig. 3, the addition of NaCl results in the atomization peak broadening and a time shift, the width of peaks depending on NaCl content. The broadening effect is related to decreasing of sputtering efficiency of Ag atoms by Na ions (atomic weight 23) in comparison with sputtering by Ar ions (atomic weight 40) in pure solution; this explanation follows from the ionic–thermal sputtering theory.^{25,29} The integral signal S_i is increased by 20–25%; it remains almost constant within the wide range of NaCl concentrations and these conditions are quite acceptable for analytical applications. Increase in S_i could be explained by reduction of ion energy and electron temperature in the presence of easily ionized atoms of Na and, as a result, by reduction of gas temperature that leads to increasing of analyte residence time.

In order to ensure high stability of the discharge and further decrease of the influence of matrix components on the atomization process, it is necessary to maintain enough flow rate of discharge gas exchange in the camera. On the other hand, extremely fast flow can induce effective removal of analyte atoms out of the optical path which results in decrease in their residence time and, correspondingly, the analytical performance of atomizer. Since the configuration of the Ar gas inlet has been changed to make possible direct gas injection into the TMHC, optimization of discharge gas flow rate is required. Table 4 demonstrates a dependence between analytical signal for Cu and Ar flow rate. It can be seen that the signal remains constant up to 120 ml min⁻¹, but at flow rates above this value the signal is decreased, which may be attributed to efficient removal of atoms by gas flow. Indeed, as is demonstrated in Table 4, comparison between convection-based residence times (τ_{conv}) at given flow rates with

Table 4 Dependence of Cu signal on Ar flow rate

S (arb.unit)	$v_{\text{Ar}}/\text{ml min}^{-1}$	$\tau_{\text{conv}}/\text{ms}$
91 ± 8	40	158.8
86 ± 8	100	63.6
93 ± 8	120	53.0
64 ± 6	200	31.8
35 ± 4	300	21.2

^a v_{Ar} corresponds to $P_{\text{Ar}} = 20$ Torr.

diffusion-based residence time at given gas pressure and temperature ($\tau_0 = 60$ ms) allows us to conclude that the removal process by gas flow becomes dominating at flow rates higher than 120 ml min⁻¹. Estimation of τ_0 was performed using a similar approach to that described in ref. 25 for $T_{\text{TMHC}} = 1600$ K, $P_{\text{Ar}} = 20$ Torr and actual dimensions of the TMHC.

Thus, these experiments have demonstrated that a TMHC atomizer provides effective decomposition of evaporated substances in a discharge plasma and, in spite of moderate NaCl influence on S_i , quantitative transfer of the analyte into atomic form, *i.e.*, background absorption was suppressed and complete atomization was achieved. After proper optimization and calibration procedures for the range of samples matrixes under investigation (such as biological fluids, industrial wastes or environmental samples) high reproducibility can be achieved.

Detection limits for standard aqueous solutions were: Cd, 1.5 pg; Cu, 10 pg; Mn, 10 pg; Pb, 12 pg; Ag, 3 pg. TMHC-ZAAS was also applied to the elemental analysis of human urine and blood.²⁵

Pulsed glow discharge in TMHC with TOF-MS detection

The results of the computer simulation include all time dependencies and space distributions for the plasma atom and ion density, as well as electrons and ion electrical current and rates of sputtering and ionization. The calculated electrical current is presented in Fig. 4, along with the experimentally measured discharge current. The voltage pulse applied to the cathode has a rectangular shape with amplitude 1.5 kV, which is equivalent to a voltage pulse of 2 kV amplitude applied to an entire discharge system with a ballast resistor. The applied voltage pulse duration is 20 µs. These parameters (including the pulse shape) were measured and entered into simulation program. As it can be seen from Fig. 4, the calculated current is in good agreement with the experiment. This is one of significant proofs that the theoretical model describes plasma processes correctly.

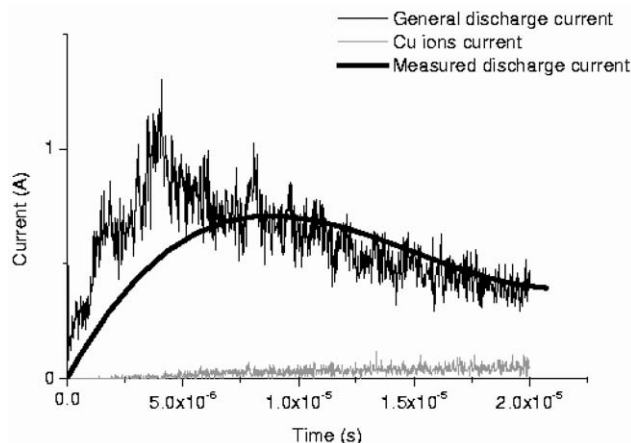


Fig. 4 Calculated profiles for total discharge current and Cu ion current. Experimentally measured discharge current is shown for comparison.

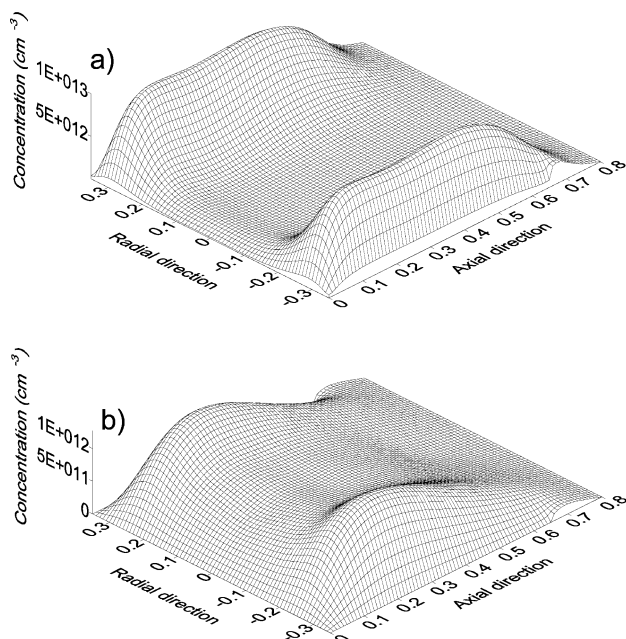


Fig. 5 Spatial 3-dimensional distribution of Cu atoms (a) and ions (b) inside TMHC and near its orifices.

Fig. 5 shows the calculated 3D spatial distribution of ions and atoms at 10 μ s after the start of the decay stage. As expected for such a short times after the end of discharge, Cu atoms are concentrated near the TMHC walls. Additionally, as can be seen, the Cu atom concentration is several times greater than Cu ions concentration near TMHC walls. During first tens of microseconds of afterglow the lower Cu ions concentration (as compared with Cu atoms concentration) can be explained by the shorter lifetime of ions near TMHC walls since the energy of ions at that time is much higher than atom's energy due to decay plasma potential.

Calculated probabilities of the loss of sample atoms and ions at the walls and probability of sample atoms Penning ionization are presented in Fig. 6(a). It can be seen that Cu atoms are mostly ionized by Penning ionization and then the ions created are transported to the walls. The diffusion loss rate of Cu atoms is high only during the first 5 μ s of afterglow, which seems to be attributed to the fact that Cu atoms are mostly located near the TMHC walls during this time (see Fig. 5) and they are efficiently lost at the walls. After that Penning ionization overwhelms all other Cu atoms loss processes.

Fig. 6(b) presents the calculated sample ions and atoms flux dynamics through the sampler orifice at afterglow. During 10–200 μ s of afterglow the Cu ion flux is several times greater than that for atoms, whereas the Cu atom concentration is several times greater than the Cu ion concentration near the TMHC walls (see Fig. 5). This difference can be explained by large Cu atom ionization probability during their diffusion time to the

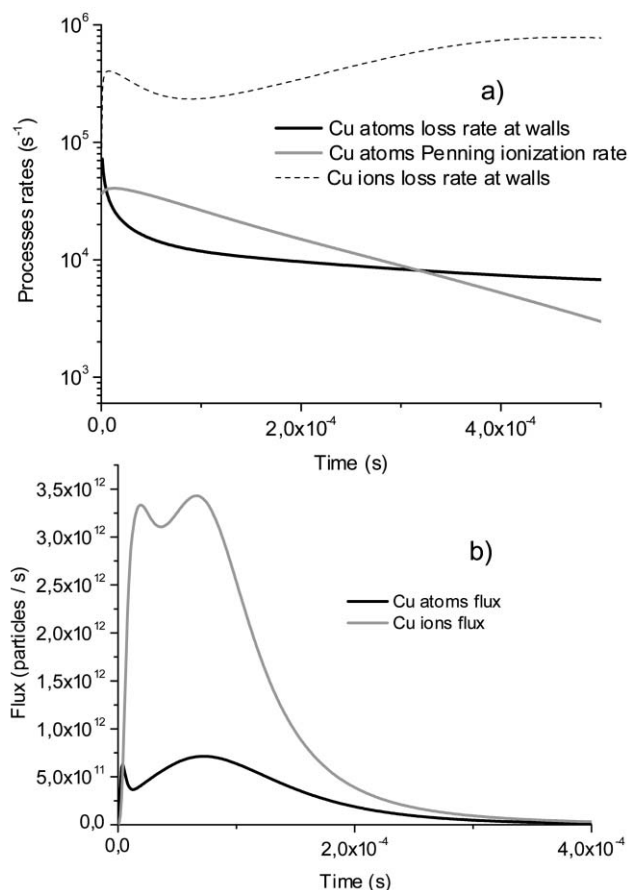


Fig. 6 (a) Sample atoms loss rate at walls, sample ions loss rate at walls and Penning ionization rate as function of time. (b) Sample atoms and ions flux through the sampler orifice.

orifice and also by the higher velocity of ions than atoms due to decay plasma potential.

To improve the sample ions transportation rate a small positive voltage (up to 20 V) was applied to the sampler. As a result this voltage produces an electrical field between the cathode and the sampler. This field accelerates ions towards the sampler. The dependence between sample ion current through the sampler orifice and applied voltage is presented in Table 5. It can be seen that the model describes this current qualitatively.

The calculations show that if a cathode bottom is plane, then the field distribution in a corner between the bottom and the cylinder surface forms a large ion flux on the cathode in this region. The flux decreases sample ion concentration in the discharge and, consequently, the intensity of the mass spectrum. Therefore the cathode with a spherical bottom was used in the experiment (see Fig. 1).

The present simulation model may be sufficiently extended by calculating a multi-pulse discharge. This will allow us to investigate the processes of residual atoms ionization,

Table 5 Ion transportation times from TMHC to repelling grid in μ s

Ion	Ar		Kr		Total time ^a	Total time ^a
	Theoretical	Experimental	Theoretical	Experimental		
	Diffusion time	Total time ^a	Total time ^a	Diffusion time	Total time ^a	Total time ^a
Cd ⁺	37	67	75 \pm 10	55	115	105 \pm 10
Cu ⁺	28	48	65 \pm 10	42	90	75 \pm 10
Nb ⁺	34	58	75 \pm 10	51	103	100 \pm 10
Ar ⁺	12	28	50 \pm 10			

^aTotal time = diffusion time + flight time, $T = 1300$ K.

temperature effects and to obtain a set of results which can be directly proved by an experiment. Moreover, some heavy elements with low ionization potential (such as Ba and Cs) may be added to the discharge. Such addition can increase the sample sputtering rate and make the discharge, degree of ionization and ions current more stable with respect to easily ionizing matrix admixtures. Furthermore, a gas flow from capillary through TMHC to sampler orifice will be included in the model.

The optimal repelling grid delay (delay between back end of discharge pulse and repelling pulse) is determined by the transportation times of the ions. These times are determined by diffusion times (from TMHC surface to orifice) and flight times (from orifice to repelling grid). In order to optimize the value of analytical signal it is reasonable to estimate transportation times for different ions. Experimental and theoretical times of optimal delay for different elements are presented in Table 5. It is obvious that different discharge gases require different grid repelling delays and total transportation time, in this case is determined as a sum of diffusion and flight times.

For estimation of the transportation times we shall estimate ion energy after the sampler. This energy is composed of two parts, the atom's motion energy and the ion's energy in the discharge. An atom beam is formed in gas-dynamic stream from an ionization area in the TMHC. In this case the atom's direct motion energy in the stream is much greater than the thermal motion energy.

It is known that Mach number reflects the relationship between the direct moving speed C_d and the thermal speed of atoms a

$$M = C_d/a = \sqrt{2/\gamma} C_d/v_m$$

where $v_m = \sqrt{2kT/m}$ is the thermal speed dispersion, T is the TMHC temperature, $\gamma = C_p/C_v$ is ratio of heat capacities (for Ar $T = 1300$ K, $v_m \approx 0.73$ km s⁻¹, $\gamma \approx 1.67$).⁴⁹

In our experimental apparatus M is approximately equal to 5, which suggests that the direct gas-dynamic speed is approximately equal to $C_d \approx 6$ km s⁻¹. This corresponds to Ar mean energy in the beam of about 10 eV.

On the other hand, the initial mean kinetic energy of Ar ions in the pulsed glow discharge is about 10 eV,⁴² which corresponds to a speed about 6.3 km s⁻¹, so the total velocity v_t is about 12.3 km s⁻¹. The average flight velocity v_a (from the sampler to repelling area) is higher than v_t because v_a is changed near the skimmer, lenses and slit. For estimation the diffusion time data from ref. 50 were used. As can be seen from Table 5, the theoretical and experimental times for different ions in Ar and Kr gases are in good agreement.

Sample sputtering dynamics is one of the most important analytical parameters because sample sputtering rate determines, to a great extent, the levels of detection limits. Figs. 7 and 8 show the samples' sputtering dynamics for Cd and Cu ions for a low average discharge current (150 mA, discharge pulse frequency $F = 1$ kHz, pulse duration 30 μ s) and for high average discharge current (3 A, $F = 8.4$ kHz, 80 μ s), respectively. As can be seen from the figures, the peaks for high average current are appreciably sharper than ones for low average current. Moreover, the addition of Ba (*i.e.*, an element with low ionization energy) to the sample causes an increase of analyte sputtering rate, as is illustrated by curves (a) and (b) in Fig. 7. This effect is determined by two factors: total ion current and sputtering ion energy.²⁵

For a high average current (Fig. 8) ion signal oscillations are observed for both Cu and Cd. Corresponding oscillation periods are different: 2.5 ms for Cu and 3.5 ms for Cd. Apparently, the oscillations are determined by the difference between frequency F and probability A of the diffusion of sample atoms from TMHC wall to sampler. In this case the

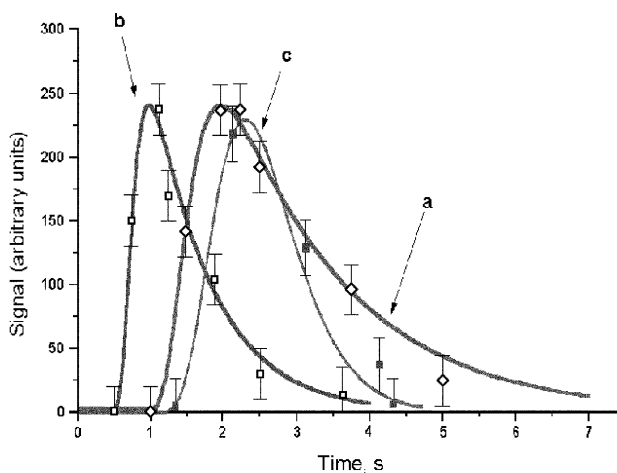


Fig. 7 Sample sputtering dynamics in TMHC-TOF-MS at low average discharge current (60 mA), Kr discharge gas. Curves are: a, 2.5 ng of Cu; b, 2.5 ng of Cu with addition of 500 ng of Ba to the sample; c, 2.5 ng of Cd.

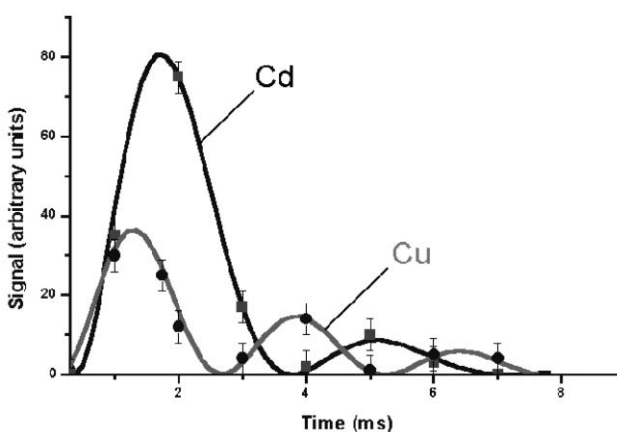


Fig. 8 Sample sputtering dynamics in TMHC-TOF-MS of 2.5 ng of Cu and Cd at high average discharge current (400 mA): Kr discharge gas.

single mass spectrum is formed from several groups of atoms sputtered from different pulses and ionized by the last pulse.

One of the difficulties in the present discharge configuration was a microcapillary discharge in the sampling capillary. This discharge appears at an Ar pressure of 0.9 Torr and capillary id of 300 μ m, and even sometimes under different conditions. In those cases the sputtering probability of the sample significantly decreased. Helium addition allowed us to eliminate microcapillary discharge. Besides, the sensitivity was increased when an Ar-He mixture was used. For example, for Ni, the addition of 1 Torr He into 0.8 Torr Ar resulted in almost 2-fold increase in ion intensities.

Standards solutions with different concentrations were used for calibration of the system. Fig. 9 shows Cd and Cu ions signals for different masses of the elements injected into a TMHC. The signals were registered under optimum experimental conditions. The reproducibility, calculated for 8 repetitive injections for the analysis of 2.5 ng Cd and 2.5 ng Cu, was equal to 0.12. Detection limits for Cd and Cu are 20 ng l⁻¹ and 15 ng l⁻¹, respectively (sample volume, 50 μ l).

Summary

The study of the pulsed TMHC glow discharge as a source of atoms and ions for analytical spectroscopy, such as ZAAS-HFM and TOF-MS, has shown that this analytical system can be successfully used for the direct analysis of liquid microsamples.

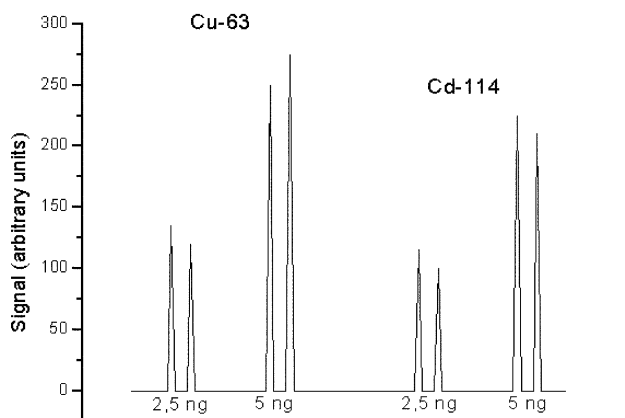


Fig. 9 Analytical determinations of Cd and Cu by TMHC-TOF-MS system.

Fast sample sputtering by ionic bombardment at moderate TMHC temperature and effective dissociation into atoms with further ionization can be achieved with pulsed GD operation.

The combination of the ZAAS-HFM system with TMHC atomizer is considered to be very promising for the manufacture of mobile spectrometers suitable for automated field and on-site analysis of samples without preparation. This system is characterized by low detection limits, low matrix effects and low discharge power and gas consumption.

As an ion source for the TOF-MS system, pulsed TMHC discharge is a very effective tool for direct atomization and ionization of liquid samples. This system can serve as a stand-alone spectrometer for element analysis or may be connected to a gas chromatograph to analyze species in complex mixtures. The work is in progress now: we expect to elucidate the analytical parameters of the TMHC-TOF-MS system for many elements and our objects will be achieved in the near future, as well as demonstrating the combination of GC with TMHC-TOF-MS.

Acknowledgements

This article was supported by grants from INTAS (Ref. No 200) for the TMHC-ZAAS system and from the Ministry of Industry, Science and Technology of the Russian Federation (2002, N32.400.112839) for the TMHC-TOF-MS system.

References

- W. W. Harrison and B. L. Bentz, *Prog. Anal. Spectrosc.*, 1988, **11**, 53–110.
- K. R. Marcus, *Glow Discharge Spectroscopies*, Plenum Press, New York, 1993.
- L. Puig and R. Sacks, *Appl. Spectrosc.*, 1989, **43**, 801–810.
- K. C. Ng, A. H. Ali and J. D. Winefordner, *Spectrochim. Acta*, 1991, **46B**, 309–314.
- W. W. Harrison, W. Hang, X. Yan and K. Ingenuity, *J. Anal. At. Spectrom.*, 1997, **12**, 891–906.
- W. W. Harrison, *Chem. Anal.*, 1988, **95**, 85–123.
- N. H. Bings, J. M. Costa-Fernandes, J. P. Guzowski Jr., A. M. Leach and G. M. Hieftje, *Spectrochim. Acta*, 2000, **55B**, 767–778.
- M. Van Straaten, K. Swenters, R. Gijbels and J. Verlinden, *J. Anal. At. Spectrom.*, 1994, **9**, 1389–1397.
- P. M. Charalambous, *Microchim. Acta*, 1987, **1**, 295–308.
- M. Saito, *Spectrochim. Acta*, 1995, **50B**, 171–178.
- D. C. Duckworth, C. M. Barshick and D. H. Smith, *J. Anal. At. Spectrom.*, 1993, **8**, 875–879.
- T. Takahashi and T. Shimamura, *Fresenius' J. Anal. Chem.*, 1994, **66**, 3274–3280.
- C. Venzago and M. Weigert, *Fresenius' J. Anal. Chem.*, 1994, **350**, 305–309.
- S. De Gent, R. Van Grieken, W. Hang and W. W. Harrison, *J. Anal. At. Spectrom.*, 1995, **10**, 689–695.
- W. Schelles, S. De Gent, K. Maes and R. Van Grieken, *Fresenius' J. Anal. Chem.*, 1996, **355**, 858.
- W. Schelles, S. De Gent, V. Muller and R. Van Grieken, *J. Appl. Spectrosc.*, 1995, **49**, 939.
- A. I. Saprykin, J. S. Becker and H.-J. Dietze, *Fresenius' J. Anal. Chem.*, 1997, **359**, 449–453.
- D. C. Duckworth, D. H. Smith and S. A. McLuckey, *J. Anal. At. Spectrom.*, 1997, **12**, 43–48.
- C. Yang, M. Mohile and W. W. Harrison, *J. Anal. At. Spectrom.*, 2000, 1255–1260.
- H. J. Kim, E. H. Piepmeier, G. L. Beck, G. G. Brumbaugh and O. I. Farmer, *Anal. Chem.*, 1990, **62**, 639–643.
- Y. Shao and G. J. Horlick, *Spectrochim. Acta*, 1991, **46B**, 165–174.
- X. Feng and G. J. Horlick, *J. Anal. At. Spectrom.*, 1994, **9**, 823–831.
- N. Jakubowski, I. Feldmann and D. Stuewer, *J. Anal. At. Spectrom.*, 1997, **12**, 151–158.
- C. G. Bruhn and W. W. Harrison, *Anal. Chem.*, 1978, **50**, 16–21.
- A. A. Ganeev and S. E. Sholupov, *Spectrochim. Acta*, 1998, **53B**, 471–486; A. A. Ganeev, M. N. Slyadnev and S. E. Sholupov, *Zh. Anal. Khim.*, 1998, **53**, 1091–1096 (in Russian).
- C. L. Chakrabarti, K. L. Headrick, P. C. Bertels and M. H. Back, *J. Anal. At. Spectrom.*, 1988, **3**, 713–723.
- F. Chen and J. C. Williams, *Anal. Chem.*, 1990, **62**, 489–495.
- B. W. Smith, N. Omenetto and J. D. Winefordner, *Spectrochim. Acta*, 1984, **39B**, 1389–1393.
- A. A. Ganeev, V. N. Grigor'yan, A. I. Drobyshev, M. N. Slyadnev and S. E. Sholupov, *Zh. Anal. Khim.*, 1996, **51**, 848–854.
- N. Jakubowski, D. Stuewer and G. Yoelg, *Spectrochim. Acta*, 1991, **46B**, 155–163.
- C. M. Barshick, D. C. Duckworth and D. J. Smith, *J. Am. Soc. Mass Spectrom.*, 1993, **4**, 47–53.
- P. A. Buger and W. Fink, *Fresenius' J. Anal. Chem.*, 1969, **244**, 314–315.
- P. H. Ratliff and W. W. Harrison, *Appl. Spectrosc.*, 1995, **49**, 863–871.
- R. C. Willoughby and R. F. Browner, *Anal. Chem.*, 1984, **56**, 2626–2631.
- M. Saito, *Anal. Chim. Acta*, 1997, **355**, 129–134.
- W. Grimm, *Spectrochim. Acta*, 1968, **23B**, 443–450.
- Glow Discharge Optical Emission Spectrometry*, ed. R. Pauling, D. Jones and A. Bengston, John Wiley and Sons, New York, 1997.
- C. L. Chakrabarti, K. L. Headrick, J. C. Hutton, P. C. Bertels and M. H. Back, *Spectrochim. Acta*, 1991, **46B**, 183–196.
- D. E. Maximov, N. K. Rudnevskii, A. K. Rudnevskii and T. M. Shabanova, *Spectral Analysis Using a Discharge in the Hollow Cathode*, Gorkii University, Gorkii, Russia, 1983.
- O. S. Lunyov and S. V. Oshemkov, *Spectrochim. Acta*, 1992, **47B**, 71–78.
- A. Bogaerts, M. van Straaten and R. Gijbels, *Spectrochim. Acta, Part B*, 1995, **50**, 179–196.
- A. Bogaerts, R. Gijbels and W. J. Goedheer, *Anal. Chem.*, 1996, **68**, 2296–2303.
- A. Bogaerts and R. Gijbels, *Anal. Chem.*, 1996, **68**, 2676–2685.
- A. Bogaerts, M. van Straaten and R. Gijbels, *J. Appl. Phys.*, 1995, **77**, 1868–1874.
- A. Bogaerts and R. Gijbels, *Anal. Chem.*, 1997, **69**, A719–A727.
- A. Bogaerts and R. Gijbels, *J. Anal. At. Spectrom.*, 2000, **15**, 895–905.
- A. Bogaerts and R. Gijbels, *J. Anal. At. Spectrom.*, 2001, **16**, 239–249.
- W. Hang, C. Baker, B. W. Smith, J. D. Winefordner and W. W. Harrison, *J. Anal. At. Spectrom.*, 1997, **2**, 143–150.
- H. Haberland, U. Buck and M. Tolle, *Rev. Sci. Instrum.*, 1985, **56**(9), 1712–1716.
- E. W. McDaniel and E. A. Mason, *The Mobility and Diffusion of Ions in Gases*, Wiley, New York, 1973.